Dalton Transactions

An international journal of inorganic chemistry

www.rsc.org/dalton

Number 21 | 7 June 2009 | Pages 4041–4260

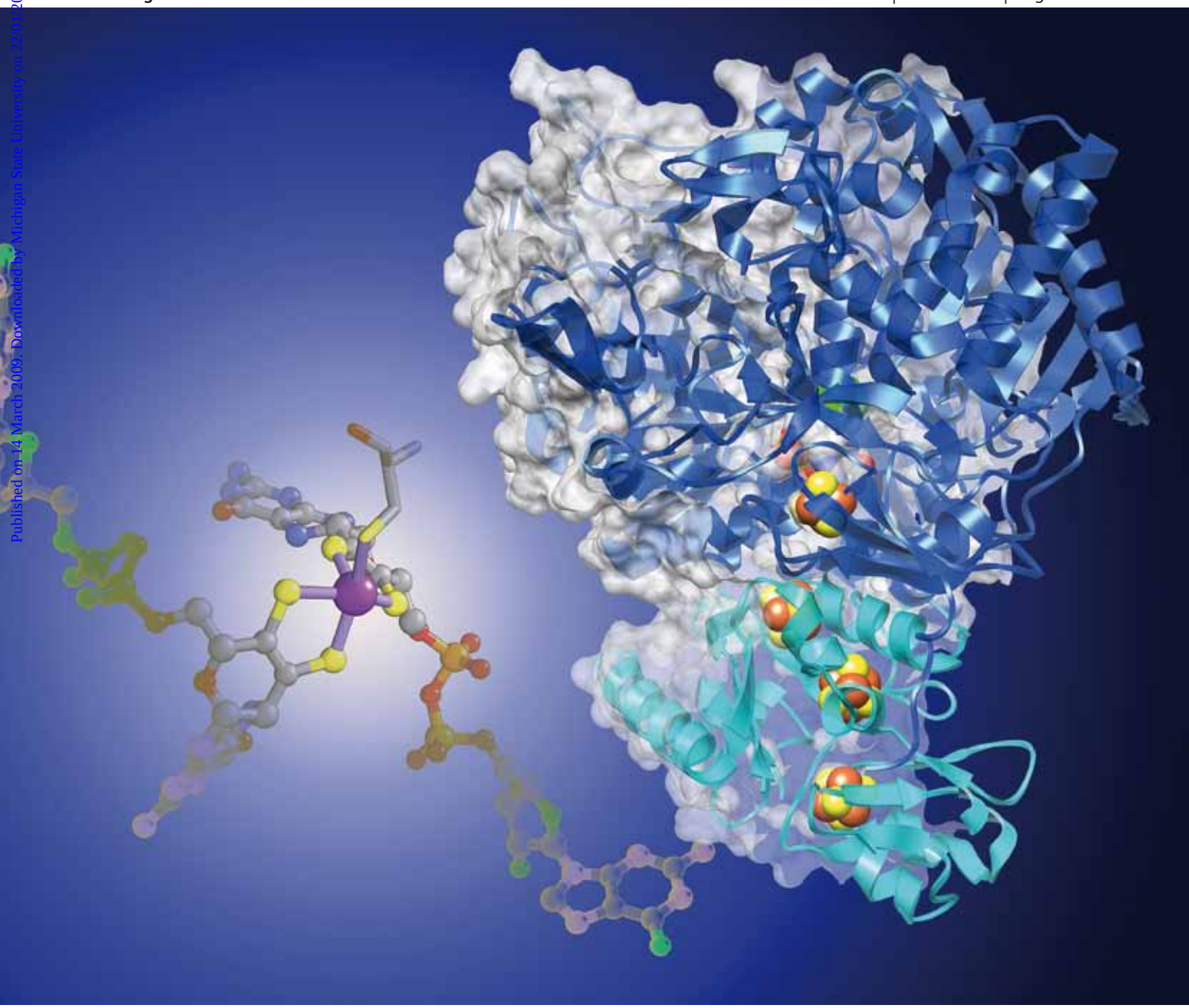

RSC Publishing

Molybdenum and tungsten enzymes: a crystallographic and mechanistic overview

Maria João Romão*

Received 25th November 2008, Accepted 20th February 2009
First published as an Advance Article on the web 14th March 2009
DOI: 10.1039/b821108f

Molybdenum and tungsten enzymes which contain the pyranopterin cofactor are ubiquitous in Nature and perform a wide variety of biological functions. They catalyze a diversity of mostly two-electron oxidation–reduction reactions crucial in the metabolism of nitrogen, sulfur and carbon. These enzymes share common structural features, but reveal different polypeptide folding topologies and different active site coordination geometries, which, in part, dictate their function and specificity. On the basis of structural, spectroscopic and biochemical characteristics, they have been classified into three broad families named according to well-studied enzymes of each family: xanthine oxidase, sulfite oxidase and DMSO reductase. An overview of the X-ray crystallography data for representative members of the three enzyme families is given here, focusing on the mechanistic implications drawn from the structural data.

1. Introduction

Molybdenum is known to be an essential trace element for animals, plants and microorganisms,[1,2,3] while tungsten is essential only for some bacteria, mostly thermophilic ones.[4,5] In animal and human nutrition molybdenum is required for the activity of several enzymes that are involved in catabolism, including the catabolism of purines and sulfur amino acids.[6,7,3] In plants, molybdenum is required in nitrate assimilation, purine metabolism, hormone biosynthesis, and most probably in sulfite detoxification.[8] In human health,[9,10] molybdenum is essential in the mechanism of action of xanthine oxidase, sulfite oxidase and aldehyde oxidase, enzymes which are involved in diseases such as gout, radical damage following cardiac failure and combined oxidase deficiency. Deficiency of the molybdenum cofactor, although rare, causes a severe disease in humans and all of the pterin-dependent enzymes (xanthine oxidase/dehydrogenase, sulfite oxidase and aldehyde oxidase) are affected. This combined enzyme deficiency has major consequences such as severe neurological abnormalities and mental retardation.[7]

With the exception of the multinuclear $MoFe_7$ cluster present in nitrogenase,[11,12] molybdenum is found in all other known molybdoenzymes in a mononuclear form, which possesses an organic tricyclic pyranopterin cofactor coordinated to the metal (Scheme 1).

The cofactor is often referred in the literature as molybdopterin or Moco (from *mo*lybdenum *co*factor), since it was originally believed to be present only in molybdenum enzymes. However, it was later found that the same form is present in tungsten enzymes.[5] Although the term molybdopterin is still often used, the alternative designation of pyranopterin is less confusing. It is coordinated to the metal *via* its dithiolene function and may be present either in dinucleotide or monophosphate form.[1] In eukaryotes the pyranopterin is found in the simplest monophosphate form (MPT). In prokaryotes it is conjugated to nucleosides, usually cytosine (MCD, molybdopterin cytosine dinucleotide) or guanosine (MGD, molybdopterin guanosine dinucleotide), and occasionally adenosine or inosine. The diversity of the pterin cofactor within known molybdenum-containing enzymes seems to be related to the species of origin rather than to the enzymatic function, as found in the enzymes studied so far. The primary role of the pterin cofactor is to position the catalytic metal (Mo or W) in the active site. In addition, it modulates the redox potential at the Mo (or W) centre and is involved, *via* the pterin ring system, in the transfer of electrons to or from other prosthetic groups.

The biosynthesis of Moco and its assembly in the molybdenum-containing enzymes invokes a rather complex pathway. Although considerable progress has been made on the enzymology of Moco biosynthesis, on the crystallography of the enzymes involved, and on the study of its regulation, there is still a lot to be discovered. It is currently a very active area of research.[13–15]

REQUIMTE-CQFB, Departamento de Química, FCT-Universidade Nova de Lisboa, 2829-516, Caparica, Portugal. E-mail: mromao@dq.fct.unl.pt

Maria João Romão

Maria João Romão obtained her PhD in 1989 at the Instituto Superior Técnico in Lisbon. As an Alexander von Humboldt post-doctoral fellow she worked with Robert Huber at the Max-Planck Institut für Biochemie in Martinsried. In this period she started to work in protein crystallography of metalloproteins, in particular molybdenum-containing enzymes, projects carried out in collaboration with the groups of José Moura and Isabel Moura in Lisbon. She is currently Associate Professor of Biochemistry and head of the protein crystallography group at the Laboratory REQUIMTE, Faculdade de Ciências e Tecnologia, Universidade Nova de Lisboa.

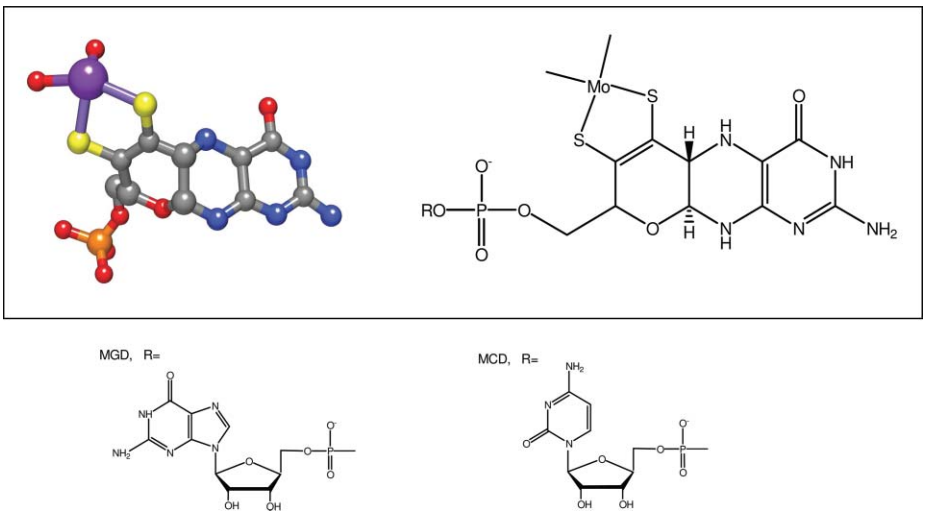

Scheme 1 The structure of the pyranopterin cofactor present in mononuclear molybdenum and tungsten enzymes. (MPT: R = H, monophosphate form; MGD: molybdopterin guanine dinucleotide; MCD: molybdopterin cytosine dinucleotide.)

2. Enzyme classification of pyranopterin-dependent enzymes

The pterin-dependent molybdenum enzymes are ubiquitous in nature and are found in almost all forms of life.[1,2,16,17] They catalyze a wide range of (mostly) redox reactions, crucial in the metabolism of nitrogen, sulfur and carbon compounds. For most of the molybdenum-dependent enzymes the catalyzed reaction is an oxo-transfer reaction coupled to electron-transfer between substrate and other cofactors such as iron–sulfur centres ([2Fe-2S] or [4Fe-4S]), hemes or flavins. In the active site, molybdenum is coordinated to the *cis*-dithiolene group of one or two pyranopterins plus additional terminal oxo/hydroxo groups and/or sulfido groups or side chains of serine, cysteine, selenocysteine or aspartate residues in a diversity of arrangements (Scheme 2).

Pyranopterin-dependent enzymes have been grouped into three broad families,[1] a classification based on X-ray structural data and supported by primary sequence alignments, spectroscopic and biochemical data: (1) The xanthine oxidase family ((one MCD or MPT) Mo^{VI} =O, =S, –OH); (2) the sulfite oxidase (and assimilatory nitrate reductases) family ((one MPT) Mo^{VI} =O, $–H_2O/OH$, (–SCys)); and (3) the DMSO reductase family ((two MGD) Mo^{VI} =O/–OH/=S/–SH, (–OSer, –SCys, –SeCys or –OAsp)). In general terms, these enzymes catalyze the transfer of an oxygen atom from water to product (or *vice versa*) in reactions that imply a net exchange of two electrons between enzyme and substrate and in which the metal ion cycles between the redox states IV and VI.

A fourth family, not represented in Scheme 2, includes the so-called "true tungstoenzymes", such as the aldehyde ferredoxin oxidoreductase (AOR) from *Pyrococcus furiosus*.[18,19] Other tungsten enzymes, such as the formate dehydrogenase from *Desulfovibrio gigas*,[20,21] belong to the DMSOR family and are highly homologous to the corresponding molybdenum enzymes.

The availability of crystal structures for several members of the three families has greatly increased our knowledge on structure and function relationships for these enzymes and given insight into the molecular and atomic details which regulate the corresponding specificities and mechanisms of catalysis. The following sections include a survey of structural and mechanistic studies based on the available X-ray crystal structures for representative members of each of the three families (Table 1).

2.1. The xanthine oxidase family

With a few exceptions, enzymes of the XO family catalyze the oxidative hydroxylation of a diverse range of aldehydes and aromatic heterocycles in reactions that involve the cleavage of a C–H and the formation of a C–O bond: $RH + H_2O \rightarrow ROH + 2H^+ + 2e^-$.

Members of this family have been found broadly distributed within eukaryotes, prokaryotes and archaea. Besides xanthine oxidase (XO)/xanthine dehydrogenase (XDH),[17,22,23] it comprises many other enzymes with diverse functions (see below). XDH is the key enzyme in the catabolism of purines, catalyzing the conversion of hypoxanthine to xanthine, and xanthine to uric acid. XDH can be converted to XO which also catalyzes the reactions of purine catabolism but is not NADH-dependent and reactive oxygen species (ROS) are formed as by-products of the reaction.[24] The closely related mammalian aldehyde oxidase is also an important enzyme involved in the metabolism of several aldehyde compounds and the biotransformation of xenobiotics.[10]

Enzymes classified in the XO family possess a $Mo^{VI}OS(OH)$ nucleus and one pyranopterin but no covalent bonding of the metal to the polypeptide chain (Scheme 2). They are organized either as homodimers of identical subunits of approximately 150 kDa, with the several redox-active cofactors placed within a single subunit (α_2), or as multi-subunit enzymes ($\alpha_2\beta_2\gamma_2$) (Table 1). In the case of the α_2 structures (xanthine oxidase and aldehyde oxidases), two spectroscopically distinguishable [2Fe-2S] centres (I and II)[25] are located in the N-terminal domain (~20 kDa), followed by the flavin domain (~40 kDa) and finally by the C-terminal catalytic domain (~90 kDa), which embeds the Moco (Fig. 1). In the simpler case of the aldehyde oxidoreductases from sulfate reducers[26] (*e.g. D. gigas*[27] and *Desulfovibrio desulfuricans* aldehyde oxidoreductases[28]), the flavin and its domain is absent and replaced by a connecting segment (Fig. 2).

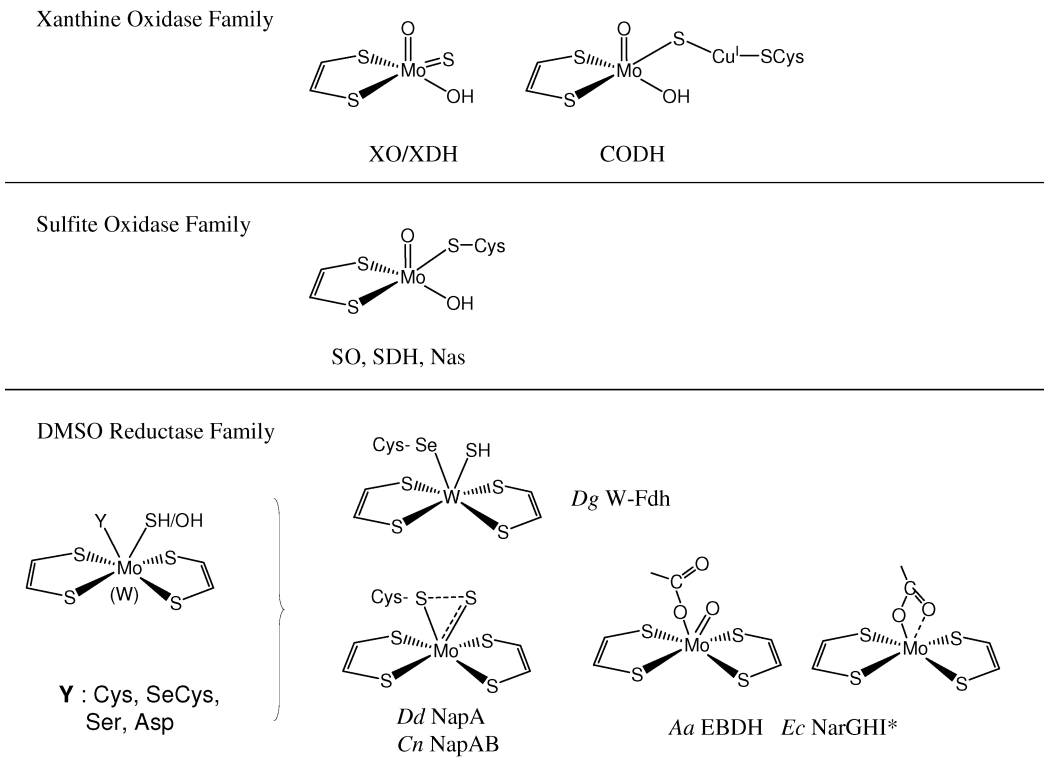

* The two independently solved structures of *Ec* NarGHI and *Ec* NarGH revealed bidentate and monodentate coordination modes of the Asp residue, respectively.

Dg: Desulfovibrio gigas; Dd: Desulfovibrio desulfuricans; Cn: Cupriavidus necator; Aa: Aromatoleum aromaticum; Ec: Escherichia coli

Scheme 2 Classification of Mo and W pyranopterin-dependent enzymes.[1]

In the multi-subunit modular enzymes, the redox centres are found within independent subunits organized as $\alpha_2\beta_2\gamma_2$ structures. The α subunit harbours the two [2Fe-2S] centres, the β subunit the flavin and the γ subunit the molybdenum cofactor. The αβγ entity associates as dimers which constitute the functional unit, similarly to the xanthine oxidase homodimer. Examples of multi-subunit enzymes are the CO dehydrogenase from *Oligotropha carboxidovorans*[29] and *Hydrogenophaga pseudoflava*,[30] the quinoline oxidoreductase from *Pseudomonas putida* 86,[31] the 4-hydroxybenzoyl-CoA reductase (4-HBCR) from *Thauera aromatica*[32,33] and the $\alpha_2\gamma_2$ 1-isoquinoline oxidoreductase from *Brevundimonas diminuta* 7.[34] The CO dehydrogenase is an interesting and unique case since it possesses a binuclear Mo/Cu active site. The 4-HBCR, a central enzyme in the anaerobic degradation of phenolic compounds, also displays unique characteristics within the XO family. The most important is the presence of an additional [4Fe-4S] cluster, which is supposed to participate in an inverted electron flow.

Crystal structures of XO-related enzymes. The first crystal structure for a xanthine oxidase-related enzyme was that of the aldehyde oxidoreductase from *D. gigas* (MOP).[27,35,36] Crystal structures of xanthine oxidase/xanthine dehydrogenases from two different sources followed: bovine milk XDH[37] and *Rhodobacter capsulatus* XDH[38] which provided additional crucial information on the tertiary structural information for this family of enzymes as well as structural details for the active sites. The overall fold and architecture of the enzymes of the xanthine oxidase family are remarkably similar. So is the arrangement of the prosthetic groups (Fig. 1 and 2) whether it is in the enzyme with a single polypeptide chain with different domains (XO/XDH, MOP) or with independent subunits (CODH, QOR) where the different cofactors are located.

The Fe/S domain (or subunit) is subdivided into 2 subdomains, each binding one of the distinct [2Fe-2S] clusters. Type I cluster is buried *ca.* 12 Å below the protein surface and its associated domain folds as a helix bundle with two central longer helices flanked by shorter ones. Its binding motif Cys-X-X-Cys-X_{33}-Cys-X-Cys is characteristic of all xanthine oxidase-related enzymes. Type II [2Fe-2S] cluster is solvent exposed and its domain fold and binding motif Cys-X_4-Cys-X-Cys-X_{12}-Cys are typical of plant and cyanobacterial ferredoxins[39] and are characteristic of the XO family of enzymes. In all structures, the molybdenum active site is located at the bottom of a 15 Å hydrophobic channel located at the interface of two subdomains of the Moco domain.

The redox centres are aligned within the protein matrix, defining a suitable intramolecular electron transfer pathway (Fig. 1 and 2), with distances between the prosthetic groups similar in all structures from the family.

The molybdenum active site of XO/XDH. In XO/XDH, the geometry of the Mo site is approximately square pyramidal with no protein ligand (Fig. 3 and Table 2). The dithiolene ring system

Table 1 Mo and W pyranopterin-dependent enzymes analysed by X-ray crystallography for representative members of the 3 families (data not exhaustive)

Enzyme	Mw/kDa	Subunit composition	Cofactors	Resol./Å	PDB code and references
Xanthine Oxidase Family					
Bovine milk XO/XDH	2 × 145	α_2	2 × ([Mo,=O,=S,-OH, MPT], 2 × [2Fe-2S], FAD)	2.5	1FIQ[37]
D. gigas AOR (MOP)	2 × 135	α_2	2 × ([Mo,=O,=O,-OH, MCD], 2 × [2Fe-2S])	1.28	1VLB[27,36]
P. putida QOR	2 × (85 + 30 + 18)	$(\alpha\beta\gamma)_2$	2 × ([Mo,=O,=S,-OH, MCD]) + (2 × [2Fe-2S]) + (FAD)	1.8	1T3Q[31]
O. carboxidovorans CODH	2 × (80 + 30 + 17)	$(\alpha\beta\gamma)_2$	2 × ([Mo-SCu,=O,-OH, MCD]) + (2 × [2Fe-2S]) + (FAD)	1.1	1N5W[29]
T. aromatica 4-HBCR	2 × (75 + 35 + 17)	$(\alpha\beta\gamma)_2$	2 × ([Mo,=O,=O,-OH, MCD]) + (2 × [2Fe-2S], [4Fe-4S]) + (FAD)	1.6	1RM6[33]
Sulfite Oxidase Family					
Chicken liver SO	2 × 50	α_2	2 × ([Mo-Cys,=O,-OH/H_2O, MPT], heme *b*)	1.9	1SOX[45]
A. thaliana SO	2 × 43	α_2	2 × ([Mo-Cys,=O,-OH/H_2O, MPT])	2.6	1OGP[49]
S. novella SDH	2 × (40 + 9)	$(\alpha\beta)_2$	2 × ([Mo-Cys,=O,-OH/H_2O, MPT]) + (heme *c*)	1.8	2BLF[47]
P. angusta Nas[a]	2 × 48	α_2	2 × ([Mo-Cys,=O,-OH/H_2O, MPT], FAD, heme *b*)	1.7	2BII[a50]
DMSOR Family					
R. sphaeroides DMSOR	88	α	([Mo-Ser,=O,$(MGD)_2$])	1.3	1EU1[61]
D. desulfuricans, NapA	83	α	([Mo-Cys,=S,$(MGD)_2$], [4Fe-4S])	1.9	2NAP[71,76]
R. sphaeroides NapAB	90 + 15	αβ	([Mo-Cys,=S,$(MGD)_2$], [4Fe-4S]) + (2 × heme *c*)	3.2	1OGY[72]
E. coli NarGHI	140 + 58 + 26	αβγ	([Mo-Asp,$(MGD)_2$], [4Fe-4S]) + (3 [4Fe-4S],[3Fe-4S]) + (2 × heme *b*)	1.9	1Q16[57]
D. gigas W-Fdh	92 + 29	αβ	([W-SeCys,=S,$(MGD)_2$], [4Fe-4S]) + (3 × [4Fe-4S])	1.8	1H0H[20,21]
E. coli Fdh-N	113 + 32 + 21	$(\alpha\beta\gamma)_3$	([Mo-SeCys,-OH,$(MGD)_2$], [4Fe-4S]) + (4 × [4Fe-4S]) + (2 × heme *b*)	1.6	1KQF[82]
A. aromaticum EBDH	90 + 30 + 20	αβγ	([Mo-Asp, acetate,$(MGD)_2$], [4Fe-4S]) + (4 × [4Fe-4S]) + (heme *b*)	1.88	2IVF[59]
P. acetylenicus acetylene hydratase	84	α	([W-Cys,-OH_2,$(MGD)_2$], [4Fe-4*S*])	1.26	2E7Z[67]
A. faecalis arsenite oxidase	92 + 14	αβ	([Mo,=O $(MGD)_2$], [3Fe-4S]) + ([2Fe-2S])	1.64	1G8J[66]

Abbreviations: XO/XDH: xanthine oxidase/dehydrogenase; AOR: aldehyde oxidoreductase; QOR: quinoline oxidoreductase; CODH: CO dehydrogenase; 4-HBCR: 4-hydroxybenzoyl-CoA reductase; SO: sulfite oxidase; SDH: sulfite dehydrogenase; Nas: eukaryotic assimilatory nitrate reductase; DMSOR: dimethyl sulfoxide reductase; Nap: periplasmic nitrate reductase; Nar: membrane bound respiratory nitrate reductase; Fdh: formate dehydrogenase; EBDH: ethylbenzene dehydrogenase.[a] X-Ray structure of the molybdenum-containing fragment.

defines the equatorial plane and contributes with two sulfur ligands, while the catalytically-essential sulfur atom occupies one of the equatorial positions. The 5-fold coordination is completed by an apical oxo group and an equatorial hydroxyl group. This OH ligand is pointing towards the funnel that leads into the active site and is the source of oxygen transferred into the substrate. In the active site, a highly conserved glutamate (Glu1261 in bovine XO) is involved in the catalytic cycle (Fig. 3, Scheme 3) being only 3.5 Å away from the metal and establishing a hydrogen bond to the hydroxyl ligand. The active site geometry is conserved in all members of the family. However, there are differences in terms of the ligands: XO/XDH and *P. putida* QOR have one sulfur and two oxygen ligands, while the AORs from sulfate reducers[28,36] and the *T. aromatica* 4-HBCR[33] have three oxygen ligands (Fig. 3). A particular case is that of *O. carboxidovorans* CODH,[29] which has an unique dinuclear Mo/Cu centre [CuSMo(O)OH].

Catalytic mechanism of XO/XDH. A model for the reductive half-reaction of the oxygen atom transfer catalyzed by xanthine oxidase-related enzymes was originally proposed on the basis of the crystal structure of MOP[27,35] and later by the structures of XO/XDH from different sources, native and complexed with inhibitors.[37,38,40–42] These structural studies, together with spectroscopic and biochemical data have led to a clarification of the reaction mechanism for the XO family of enzymes. Mechanistic studies and proposals for the reaction mechanism of xanthine oxidase have been recently reviewed by Hille *et al.*[23,43] and by Nishino *et al.*[24]

In MOP, the location of the inhibitor isopropanol present in the second coordination sphere of molybdenum was proposed as the putative substrate binding site,[27,28] while in the bovine milk XO structure, its position is replaced by the competitive inhibitor salicylate[37] (Fig. 3). In both structures, well-ordered, catalytically-relevant water molecules are found in the active site cavity.

The main aspects of this mechanism (Scheme 3) are: (a) a coordinated OH ligand is activated by the neighbouring conserved glutamate residue (Glu1261 in bovine XO) and is transferred onto the substrate. This nucleophilic attack is facilitated by hydrogen bonding interactions of the substrate molecule with conserved residues of the active site cavity as well as conserved internal water molecules. (b) The resulting intermediate, generated after hydride transfer to the sulfido group, replaces the coordinated OH at the molybdenum. (c) The product is released from the reduced molybdenum centre and a water molecule reoccupies the vacant coordination position. In terms of the orientation mode of the hypoxanthine and xanthine substrate molecules when being hydroxylated, Pauff *et al.*[43] and Yamagushi *et al.*,[44] have different proposals, although keeping the essential features of the reaction mechanism (A and B, respectively, in Scheme 3). This also implies different roles for some of the conserved amino acid residues in

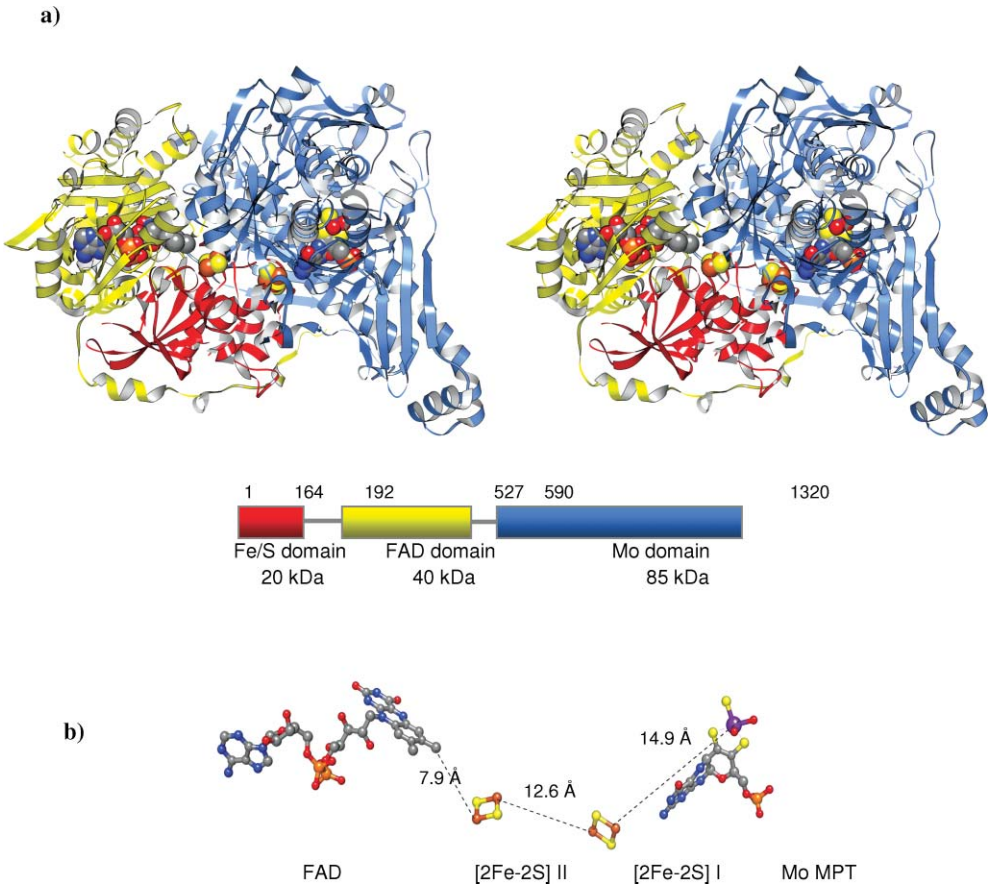

Fig. 1 (a) Stereo view of the crystal structure of bovine milk xanthine oxidase[37] and schematic representation of the domain structure with respect to the primary sequence. (b) Arrangement of the metal cofactors involved in electron transfer: Mo MPT, [2Fe-2S] I, [2Fe-2S] II and FAD, colour-coded as atom types.

the active site pocket. In order to clarify these aspects, additional high resolution crystal structures of complexes with substrates or analogues are needed. However, in several of the crystallographic studies it is found that, even at resolutions higher than 2.0 Å, the exact binding mode cannot be precisely determined, probably reflecting a mixture of possible orientations.[24]

The two reducing equivalents generated in the course of the reaction are transferred to an external electron acceptor and the electron flow in and out of the molybdenum centre is mediated by the pterin cofactor to the closest [2Fe-2S] I centre (*ca.* 12 Å) and from this to the exposed centre [2Fe-2S] II.

2.2. The sulfite oxidase family

The members of this family include not only sulfite oxidizing enzymes found in plants, animals and bacteria but also the assimilatory eukaryotic nitrate reductases.[7] These assimilatory nitrate reductases catalyze the first and rate-limiting steps of nitrate assimilation in plants, algae and fungi, and are totally different from the bacterial nitrate reductases with respect to primary and tertiary structures. The latter belong to the DMSO reductase family of molybdenum enzymes and are considered in the next section.

There are three different sulfite-oxidizing enzymes presently known: sulfite oxidase (SO) in animals, SO in plants, and sulfite dehydrogenase (SDH) in bacteria. Structural, spectroscopic and biochemical studies carried out in sulfite-oxidizing enzymes have been recently reviewed by Feng *et al.*[7] In animals SO catalyzes the physiologically-vital oxidation of sulfite to sulfate, with cytochrome *c* as the physiological electron acceptor. This reaction is the final step in the oxidative degradation of the sulfur-containing amino acids cysteine and methionine and is critical in detoxifying excess sulfite. Human SO deficiency is a fatal genetic disorder that leads to early death, and impaired SO activity is implicated in sulfite neurotoxicity.[45] The plant SO is responsible for detoxifying excess sulfite produced during sulfur assimilation. It has been shown that *Arabidopsis thaliana* SO uses oxygen as the terminal electron acceptor.[46] The *Starkeya novella* SDH has an important role in converting sulfite formed during dissimilatory oxidation of reduced sulfur compounds, and cannot transfer electrons to molecular oxygen.[47]

Enzymes within this family typically have one molybdopterin cofactor (MPT) and a $Mo^{VI}OOH$ nucleus. The polypeptide chain coordinates directly to the molybdenum site by a cysteinyl residue (Scheme 2). With the exception of plant SO, which contain only Moco, all sulfite oxidizing enzymes, possess two redox centres: Moco and a heme cofactor. They form dimeric structures. The animal SOs are homodimeric and bind Moco and one *b*-type heme in different domains (Fig. 4 and Table 1). The plant SOs are also homodimeric, but have only the Moco domain. The

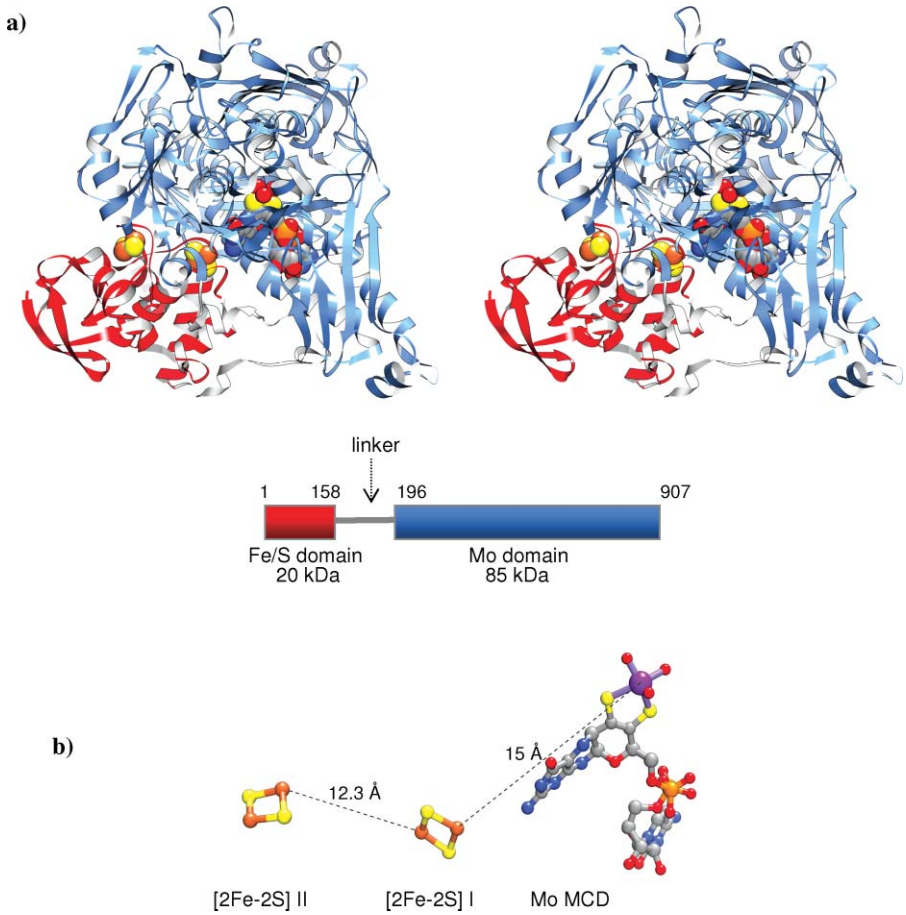

Fig. 2 (a) Stereo view of the crystal structure of the *D. gigas* aldehyde oxidoreductase (MOP)[27,36] and schematic representation of the domain structure in respect to the primary sequence. (b) Arrangement of the metal cofactors involved in electron transfer: Mo MCD, [2Fe-2S] I, [2Fe-2S] II, colour-coded as atom types.

bacterial enzyme SDH is heterodimeric (SorAB) and contains Moco and one *c*-type heme in independent subunits. Intraprotein interdomain electron transfer occurs between the two centres and is critical for the enzymatic turnover.

Crystal structures of sulfite-oxidizing enzymes. Most of the knowledge about this family of enzymes derives from structural studies on the chicken liver SO.[45,48] X-Ray structures are also available for the other types of enzymes: *A. thaliana* SO[49] and *S. novella* SDH.[47] The crystal structure of the molybdenum-containing fragment (residues 1–484) of the assimilatory nitrate reductase from *Pichia (P.) angusta* has also been reported.[50]

Chicken SO is a α_2 dimer and each monomer has three domains: the first domain (9 kDa) binds a *b*-type heme, the second is the Moco domain of approximately 25 kDa and a third 15 kDa domain is involved in the contact between the 2 monomers (dimerization domain) (Fig. 4). The heme domain is structurally similar to bovine cytochrome *b*5 while the Moco domain has a novel fold typical of the SO-related enzymes. The molybdenum and heme domains are linked by a 10 amino acid flexible loop and the Mo–Fe distance is 32 Å.[45] This large distance between the two metal centres could not be expected to allow efficient electron transfer and this was interpreted as a "redox-inactive" state. However, intramolecular electron transfer between the two centres can be very fast and one possible explanation is that chicken SO may adopt different conformations in the crystal and in solution, where the heme and molybdenum centres could be brought much closer, involving substantial conformational changes of the corresponding domains.[51,52]

The *S. novella* SDH is a heterodimer consisting of a large molybdenum-binding subunit (SorA, 40 kDa) and a small heme *c* subunit (SorB, 9 kDa). The crystal structure of this enzyme revealed a different relative positioning of the two domains and respective metal centres, which are much closer (Mo–Fe distance ~16 Å) in comparison to chicken SO, enabling a direct electron transfer pathway between the two redox centres to be postulated.[47] Bacterial SDH can thus be a suitable model to study electron transfer in sulfite oxidizing enzymes.

The molybdenum active site of sulfite oxidase. In the crystal structure of chicken SO[45] the Mo atom is coordinated by five ligands with pseudo square pyramidal coordination geometry (Fig. 5, Table 2). A terminal oxo ligand occupies the axial position while the equatorial positions are occupied by three sulfur atoms (two from the pterin dithiolene and one from a conserved cysteine) and by a hydroxo/water ligand. In spite of the variability in the overall structures and presence of additional cofactors, the active sites of chicken SO, *A. thaliana* SO,[49] *S. novella* SDH[47] and

Table 2 Geometry of the active site for representative members of each family. Mo/W–ligand bond distances given in Å, and in parentheses the resolution of the corresponding structures

Xanthine oxidase family						
Bovine milk XO/XDH[42] (1.98 Å)						
Mo–OH	Mo–O (apical)	Mo–S (equatorial)	Mo–S1 (MPT)	S2 (MPT)		
1.97	1.73	2.17	2.42	2.44		
D. gigas AOR[36] (1.28 Å)						
Mo–OH	Mo–O1 (apical)	Mo–O2	Mo–S1 (MCD)	Mo–S2 (MCD)		
1.99	1.74	1.79	2.41	2.49		
Sulfite oxidase family						
Chicken liver SO[45] (1.9 Å)						
Mo–OH/H_2O	Mo–O	Mo–S(Cys185)	Mo–S1 (MPT)	Mo–S2 (MPT)		
2.25	1.74	2.47	2.38	2.37		
DMSOR family						
D. desulfuricans Nap[76] (1.9 Å)						
Mo–S	Mo–S(Cys140)	S–S(Cys)	Mo–S1 (MGD^{810})	Mo–S1 (MGD^{810})	Mo–S1 (MGD^{811})	Mo–S1 (MGD^{811})
2.26	2.34	2.38	2.40	2.42	2.48	2.46
D. gigas W-Fdh[84] (1.8 Å)						
W–S	W–Se(SeCys158)	W–S1 (MGD^{810})	W–S1 (MGD^{810})	W–S1 (MGD^{811})	W–S1 (MGD^{811})	
2.42	2.55	2.37	2.48	2.50	2.38	
E. coli formate-reduced Fdh-H[84] (2.3 Å)						
Mo–S	Mo–SeCys140	Mo–S1 (MGD^{810})	Mo–S1 (MGD^{810})	Mo–S1 (MGD^{811})	Mo–S1 (MGD^{811})	
2.1	Unbound	2.23	2.27	2.49	2.29	

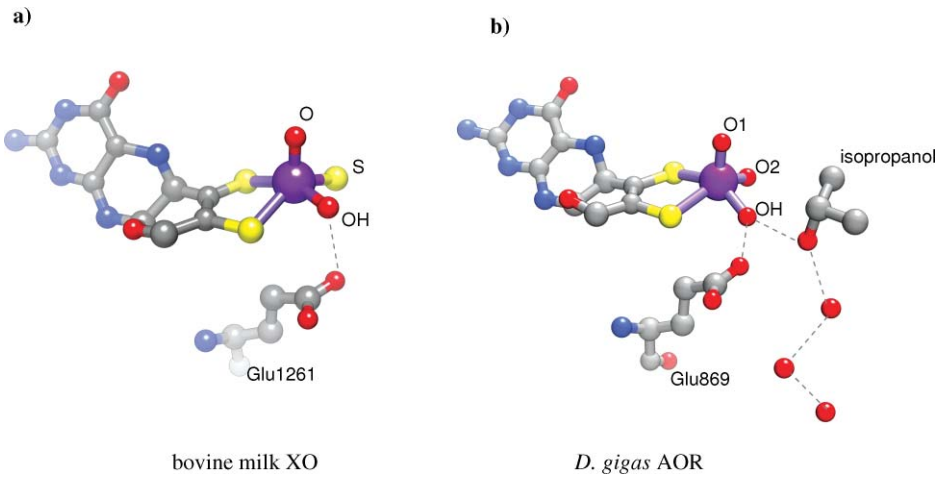

Fig. 3 (a) The Mo active site of bovine milk xanthine oxidase [Mo,=O,=S,-OH, MPT] and the conserved glutamate 1261.[41] (b) The Mo active site in the inhibited structure of the *D. gigas* aldehyde oxidoreductase [Mo,=O,=O,-OH, MCD], the conserved glutamate 869 and the inhibitor isopropanol, which is held by hydrogen bonds to the OH ligand and to 3 conserved, buried water molecules.[36]

P. angusta Nas[50] show a remarkable conservation of the active site coordination geometry, as well as of the active surrounding residues.

Catalytic mechanism of sulfite oxidase. The active site of sulfite oxidase is deeply buried in the protein and is lined by highly conserved amino acid residues (Arg138, Arg190, Arg450, Trp204 and Tyr322 in chicken SO), and the three arginines create a rather positively charged cavity (Fig. 5). The crystal structure of chicken SO has been determined in the free and sulfate-bound forms.[45,48]

The general mechanism, originally proposed by Hille[53] based on the reaction of model Mo(VI)O_2 compounds, is still the currently accepted one. The sulfite molecule is oxidized to sulfate at the molybdenum centre and the reducing equivalents are transferred to the heme *b*. The terminal electron carrier is exogenous cytochrome *c* which is reduced. The reaction mechanism involves initial nucleophilic attack of SO_3^{2-} to the electrophilic equatorial

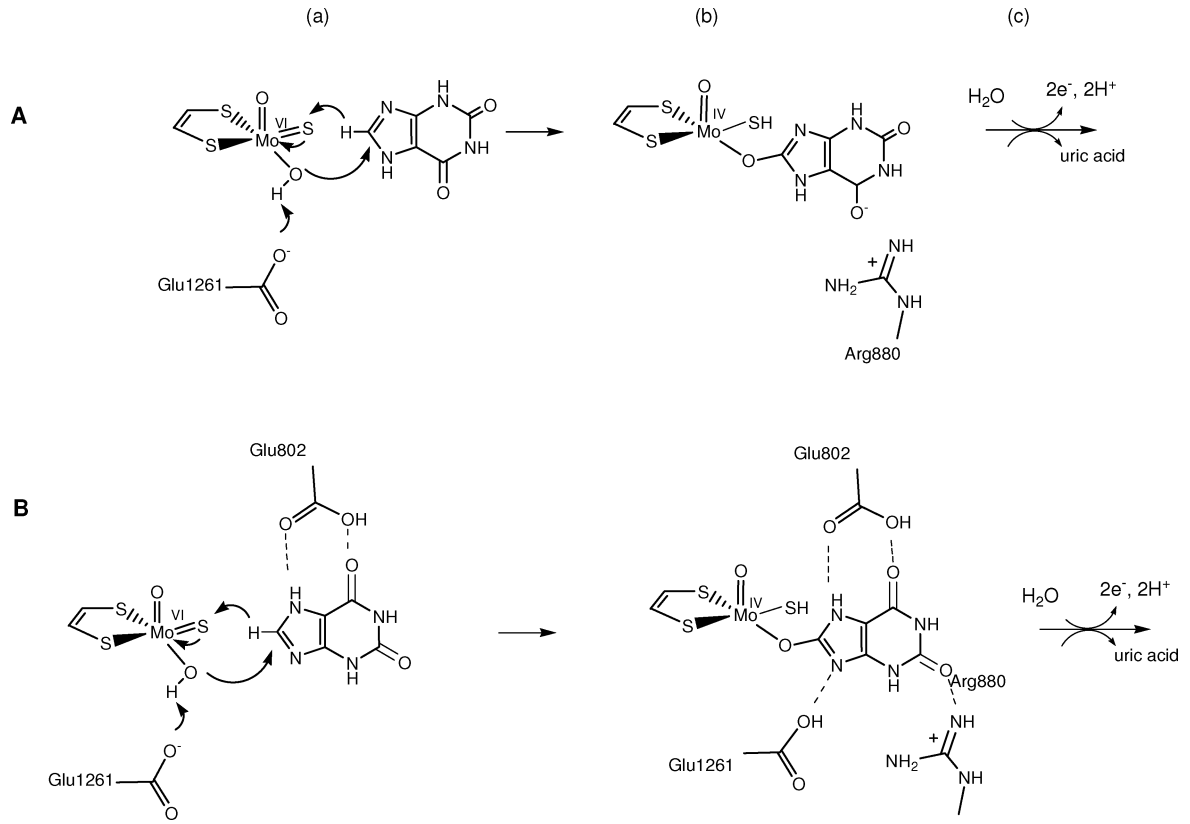

Scheme 3 Reaction mechanism of xanthine oxidase and different binding modes of the substrate xanthine as proposed (A) by Pauff *et al.*[43] and (B) by Yamaguchi *et al.*[44] The different orientation of the substrate proposed by each group of authors implies different mechanistic roles for the conserved amino acids of the active site region. The numbering is that of bovine milk xanthine oxidase.

oxo group of **1** (Scheme 4), generating a transient two-electron reduced oxo-Mo(IV) sulfate species (**2**). A hydrolysis reaction releases SO_4^{2-} and completes the oxygen atom transfer reaction, generating species **3** and completing the cycle.

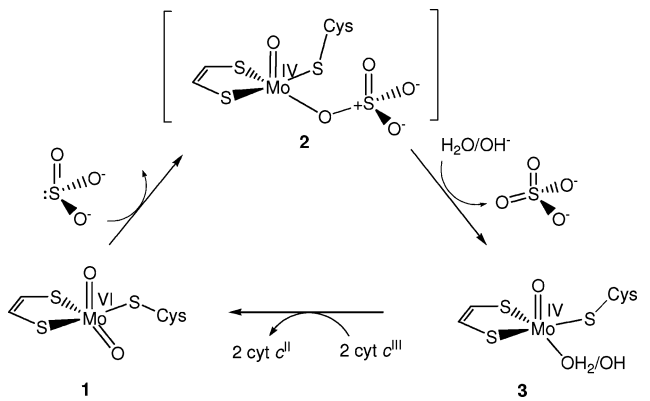

Scheme 4 Proposed catalytic mechanism for sulfite-oxidizing enzymes.[53]

2.3. The DMSO reductase family

The dimethyl sulfoxide (DMSO) reductase family of molybdenum (and tungsten) enzymes is a considerably larger and more diverse one compared to the other two. It has been divided into subfamilies I, II and III.[54,55] Its members are found in bacteria and archaea and include diverse enzymes such as dissimilatory nitrate reductases and formate dehydrogenases[56] (subfamily I); respiratory nitrate reductases I[57,58] and ethylbenzene dehydrogenase (EBDH)[59] (subfamily II); DMSO reductase[60,61] and trimethylamine N-oxide (TMAO) reductase[62,63] (subfamily III). Unique members of this family are the arsenite oxidase[64–66] and the W-containing acetylene hydratase.[67]

With the exception of formate dehydrogenases, members of the DMSOR family catalyze the transfer of an oxygen atom to or from a lone electron pair of the substrate. Unique cases are the W acetylene hydratase from *Pelobacter acetylenicus*, which catalyzes a non-redox reaction, the hydration of acetylene to acetaldehyde, as part of an anaerobic degradation pathway of unsaturated hydrocarbons[67] and the arsenite oxidase from *Alcaligenes faecalis* NCIB 8687, involved in the detoxification of arsenic, oxidizing $As^{III}O_2^-$ (arsenite) to the relatively less toxic $As^{V}O_4^{3-}$ (arsenate). Though there is a high structural similarity with other members of the family, its active site presents unique features since it lacks an amino acid side chain coordinating the W atom.

The crystal structures of enzymes of the DMSOR family show a high degree of similarity in the overall fold. However, there is considerable variation in the structure of the molybdenum (or tungsten) active site, not only at the metal coordination sphere, but also with the surrounding amino acid residues. These subtle, but important, local differences at the catalytic sites of the different enzymes contribute to the remarkable diversity of functions performed by enzymes of the DMSOR family. At the active site, the metal atom is coordinated by two pterin cofactors,

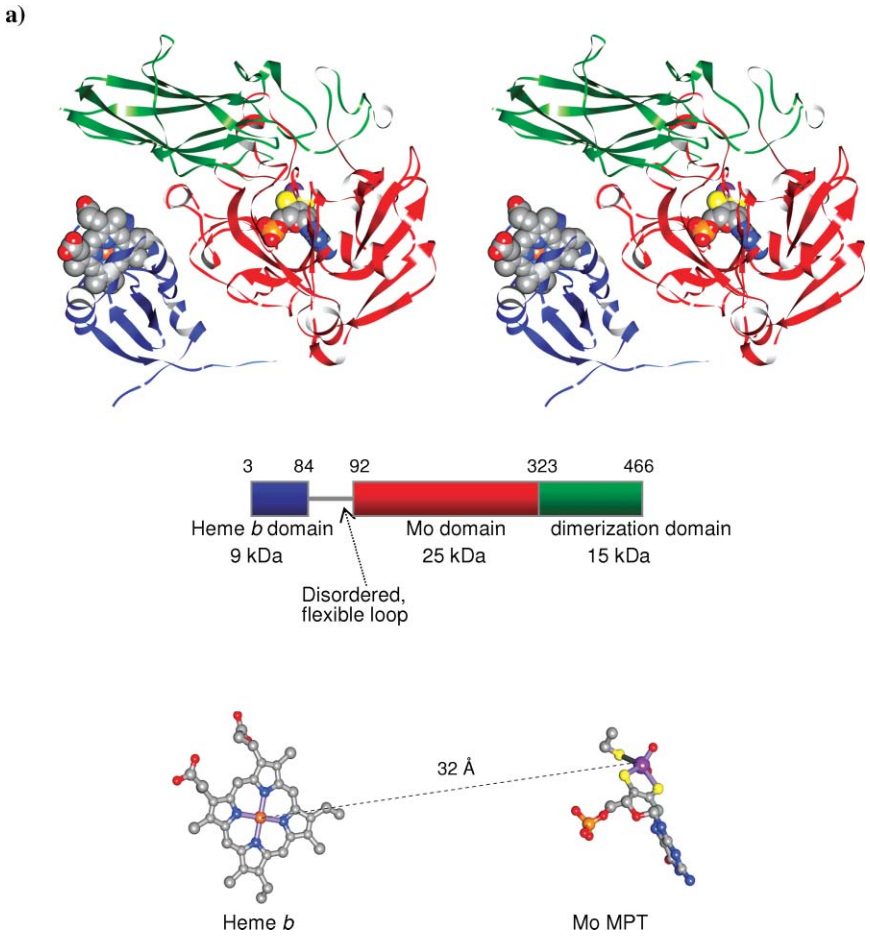

Fig. 4 (a) Stereo view of the crystal structure of chicken liver sulfite oxidase[45] and schematic representation of the domain structure with respect to the primary sequence. (b) Arrangement of the metal cofactors: Mo MPT and heme *b*, colour-coded as atom types.

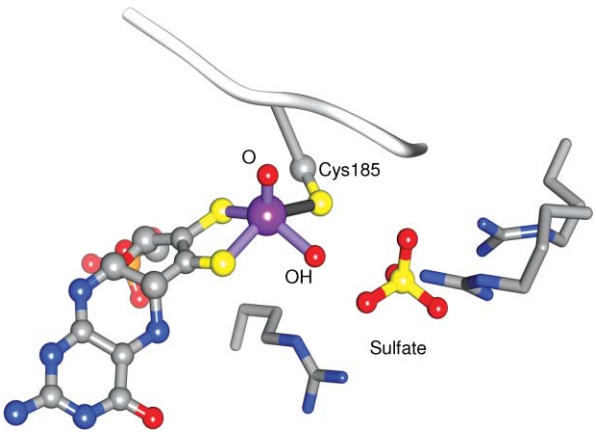

Fig. 5 The Mo active site of chicken liver sulfite oxidase [Mo-Cys,=O,-OH/H_2O, MPT] complexed with sulfate in the active site.[45]

present as guanine dinucleotide moieties (MGD), and different types of ligands as shown in Scheme 2. The amino acid which coordinates the molybdenum atom differs among the several enzymes of the family: cysteine in periplasmic dissimilatory nitrate reductase and acetylene hydratase, selenium-cysteine in formate dehydrogenase, aspartate in the membrane-bound respiratory nitrate reductases and ethylbenzene dehydrogenase and a serine in DMSO reductase.[56] Only arsenite oxidase has no ligand from the polypeptide chain. Formate dehydrogenases are one of the few enzymes capable of incorporating either molybdenum or tungsten at their active sites.

The first crystal structures reported for a member of this family were those of the DMSO reductase from *Rhodobacter sphaeroides*[61] and from *R. capsulatus*.[60] Our knowledge of this family has been highly increased due to numerous structural and spectroscopic studies of nitrate reductases and formate dehydrogenases from different bacterial sources.[26,56,68] These have included not only several crystallographic analyses of native and inhibited forms of the enzymes, but also biochemical, spectroscopic and computational studies. The information provided by the different techniques has contributed to a clarification of the reaction mechanisms involved.

The next sections are focused on structural and mechanistic results on periplasmic nitrate reductases and formate dehydrogenases.

Nitrate reductases: crystallographic studies. Nitrate reductases catalyze the reduction of nitrate to nitrite according to the reaction:

$$NO_3^- + 2H^+ + 2e^- \rightarrow NO_2^- + H_2O,\ E^\circ = 420\ \text{mV}$$

With the exception of the eukaryotic assimilatory nitrate reductases from the SO family, all other nitrate reductases belong to the

DMSOR family, but are organism-dependent, with differences in their cell location, metabolic path where they participate and catalytic centre (Scheme 2 and Table 1). They are of bacterial origin and comprise the periplasmic dissimilatory nitrate reductases (Nap), the cytoplasmatic assimilatory nitrate reductases (Nas) and the membrane-bound respiratory nitrate reductases (Nar).[56,69,70]

Crystal structures are available for four different periplasmic nitrate reductasesm,[71,72,73,74] as well as for the membrane-bound nitrate reductase from *Escherichia coli* NarGHI.[57,58] The Nar crystal structure revealed novel aspects, in particular the presence of an aspartate side chain as a ligand of molybdenum present in two binding modes. The 3D structures of the catalytic subunits of all these structures are very similar in terms of metal cofactor content, global fold, and domain organization. However, in the region close to the active site, as well as in the funnel that provides access to the molybdenum centre, there are differences between Nap and Nar.

The discussion that follows is focused on the periplasmic nitrate reductases. With the exception of the simplest monomeric NapA from *Desulfovibrio desulfuricans* ATCC, periplasmic nitrate reductases are usually found in association with a smaller subunit (~17 kDa) (NapB), containing 2 *c*-type hemes, involved in the transfer of electrons.

The first Nap structure to be solved (1.9 Å resolution) was that of the monomeric *D. desulfuricans* NapA[71] (Fig. 6). In 2003, Arnoux *et al.*[72] reported a low resolution (3.2 Å) structure of the NapAB complex from *R. sphaeroides* and in 2007, Jepson *et al*[73] described the 2.5 Å resolution structure of the *E. coli* NapA. The recently reported crystal structure of NapAB from *Cupriavidus necator*[74] has been solved to atomic resolution (1.5 Å). In all structures, the residues at the active site cavity and at the funnel which leads to it are conserved, as well as those involved in the Mo-bis(MGD) and [4Fe-4S] binding. The catalytic subunit NapA (70–90 kDa), contains a bis(MGD) cofactor and one [4Fe-4S] center. In the oxidized form, the active site is formed by a distorted hexa-coordinated Mo(VI) ion, in which the metal atom is coordinated by four sulfur atoms from two dithiolene ligands (MGD), one sulfido ligand, and a cysteinyl ligand from the protein. The NapA molecule is organized into four domains, three of which are formed by non-contiguous stretches of the polypeptide chain. Amino acid residues from all four domains are involved to variable extents in the $Mo(MGD)_2$ cofactor binding which extends across the interior of the protein structure. The spatial arrangement of two of the domains defines a funnel-like cavity at their interface, allowing access to the molybdenum centre. This 15 Å deep channel is coated with a few charged residues (Arg354, Asp155, Glu156 in *D. desulfuricans* NapA numbering) creating a favourable environment for binding and orienting the charged substrate molecule.

The molybdenum atom is located at the bottom of the channel and is 12 Å away from the nearest Fe of the [4Fe-4S] cluster. The latter is located at the periphery of the molecule and contacts one of the MGD cofactors *via* a conserved Lys residue, through the

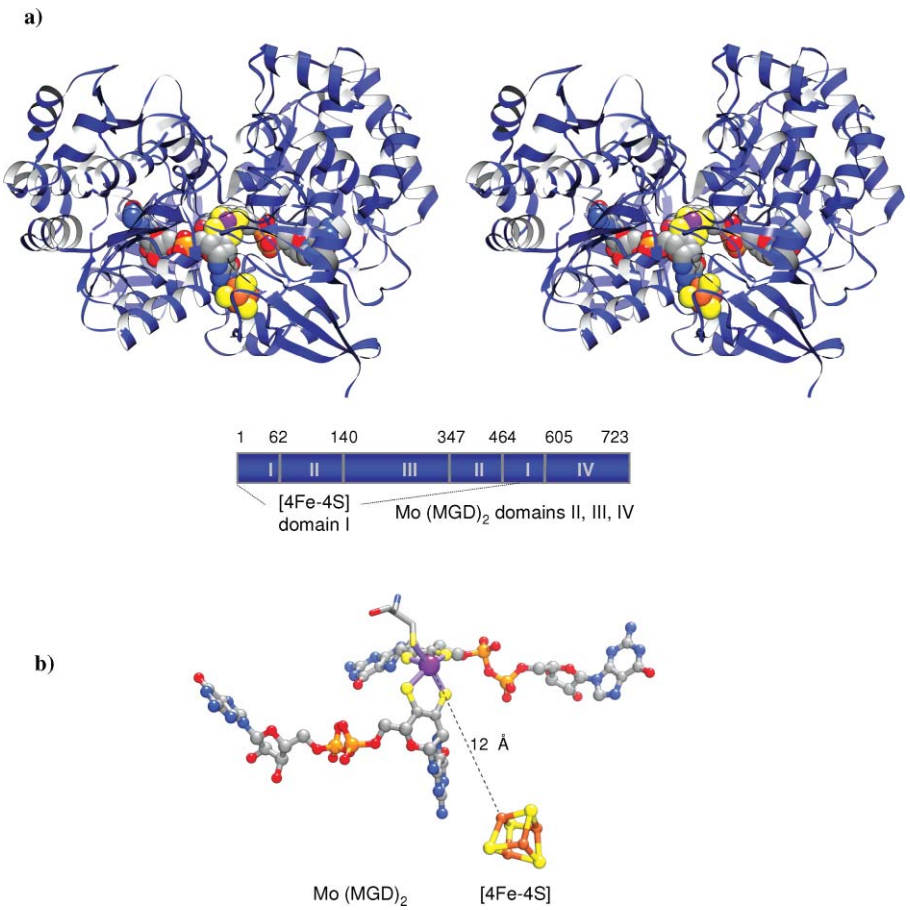

Fig. 6 (a) Stereo view of the crystal structure of the *D. desulfuricans* periplasmic nitrate reductase NapA[71,76] and schematic representation of the domain structure with respect to the primary sequence. (b) Arrangement of the metal cofactors: Mo $(MGD)_2$ and [4Fe-4S], colour-coded as atom types.

exocyclic NH_2 of the pterin ring. The importance of that lysine residue has been proven by mutagenesis studies of NapAB from *C. necator*.[75] Interestingly, this electron transfer pathway and the involved lysine are conserved in formate dehydrogenases. In Nar, there is a similar electron transfer path but the position of the Lys is replaced by an Arg residue, conserved in the Nar subfamily.

The molybdenum active site of periplasmic nitrate reductases. In the native oxidized form of Nap the Mo atom is co-ordinated by six sulfur ligands in a distorted trigonal prismatic geometry (Fig. 7 and Table 2). Four ligands are from the two 1,2-ene-dithiolate sulfur atoms of the MGD cofactors with Mo–S bond distances ranging from 2.33–2.44 Å (Table 2). A fifth sulfur ligand is the side chain of a cysteine residue and the sixth ligand is also a sulfur atom. This sixth ligand was originally interpreted in the enzyme from *D. desulfuricans* as a hydroxyl/water molecule (Mo–O distance ~2.1 Å).[71] However, new crystallographic studies of *D. desulfuricans* Nap and *C. necator* NapAB allowed a more detailed and clear picture of the molybdenum active site and gave very strong evidence that the sixth Mo ligand is a sulfur atom instead.[76] In addition, the distance between the sulfur ligand and the Sγ of the coordinating cysteine is substantially shorter than the van der Waals contact distance and varies between 2.2 Å and 2.85 Å (in seven structures analyzed), indicating a partial disulfide bond (Table 2 and Fig. 7). The two other crystal structures of related enzymes (*R. capsulatus* NapAB[72] and *E. coli* NapA[73]) were not solved to high enough resolution (3.2 Å and 2.5 Å, respectively) to allow a clear definition of the active site. The crystal structure of *C. necator* NapAB,[74] solved to nearly atomic resolution (1.5 Å), revealed the same coordination sphere as *D. desulfuricans* NapA.

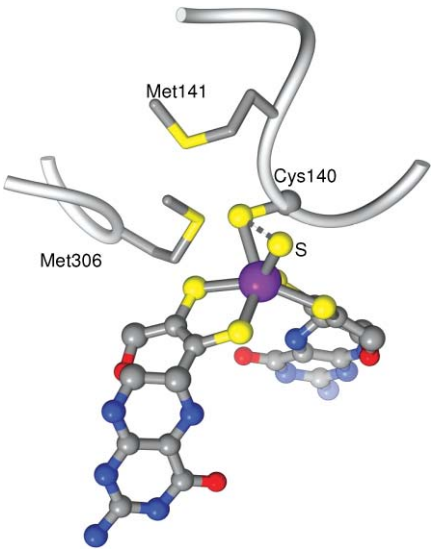

Fig. 7 The Mo active site of *D. desulfuricans* periplasmic nitrate reductase [Mo-Cys140,=S,$(MGD)_2$] and conserved methionines Met141 and Met306 of the active site.

This new coordination motif had never been proposed for a member of the DMSOR family of molybdenum enzymes and led to a revision of the reaction mechanism for periplasmic nitrate reductases.

Catalytic mechanism of periplasmic nitrate reductases. The catalytic mechanism for the reduction of nitrate to nitrite was originally proposed on the basis of the *D. desulfuricans* NapA crystal structure reported in 1999,[71] and has been generally accepted. In that mechanism, the substrate molecule would bind directly to the Mo(IV) ion in the vacant position left by the hydroxyl ligand. Two electrons would then be transferred from molybdenum to the nitrate molecule with simultaneous release of nitrite and regeneration of the Mo(VI) from of the enzyme. In the light of the new findings of an unexpected sulfur ligand in the coordination sphere, the reaction mechanism had to be revised and three hypothetical alternative mechanisms were proposed as depicted in Scheme 5.[76] The new proposals take into account molybdenum and ligand-based redox chemistry, instead of the currently accepted view of the redox role performed by the molybdenum atom alone. In that work, it has been considered that the (partial) formation of a S–S bond can influence the reduction of Mo(VI) to Mo(IV). Such a redox interplay of molybdenum and sulfur was in fact suggested for the first time in 1980 by Stiefel *et al.*[77,78] for related model compounds.

The mechanistic alternative involving intermediate (i), implies that the Cys ligand would disconnect from the molybdenum atom leaving space for the direct binding of the substrate molecule to the Mo. This putative mechanism is related to that proposed for the *E. coli* Fdh-H (*cf.* next section) and is supported by the lack of detection of hyperfine coupling with the non-solvent exchangeable methylene protons from the Cys ligand.[79] Alternative (ii) implies the formation of an adduct Mo–S–ONO_2^- and implies a ligand-based redox chemistry. Alternative (iii) would involve the direct coordination of the nitrate ion in a seventh coordinating mode, as suggested by EXAFS data for *Paracoccus pantotrophus* Nap, which shows hepta-coordinated molybdenum sites in several forms of the enzyme.[80] To differentiate between the possible alternatives further structural data of different forms of the enzyme complemented with spectroscopic and computational tools are necessary.

Formate dehydrogenases: crystallographic studies. Formate dehydrogenases catalyze the oxidation of formate to carbon dioxide, according to the reaction:

$$HCOO^- \rightarrow CO_2 + H^+ + 2e^-,\ E^\circ = -420\ mV$$

Until now, three formate dehydrogenases (Fdh) have been characterized by X-ray crystallography: The *E. coli* Fdh-H, one of the components of the formate hydrogen lyase complex in *E. coli*,[81] the *E. coli* membrane bound Fdh-N, which participates in the redox loop of the proton motive force generation across the membrane,[82,83] and the tungsten-containing Fdh from the sulfate reducer *D. gigas*.[20,21] The *E. coli* Fdh-H is a simple monomeric enzyme (79 kDa) containing one molybdenum active site and one [4Fe-4S] cluster and the crystal structures of both oxidized (2.8 Å resolution) and formate-reduced (2.3 Å resolution) forms were reported.[81] The *E. coli* Fdh-N is a very large (~500 kDa) heterotrimeric complex $\alpha_3\beta_3\gamma_3$ with subunits of 113, 32 and 21 kDa, respectively.[82] The catalytic α subunit is considerably larger than that of Fdh-H but the core 3D structures are quite similar. The W-Fdh from *D. gigas* is a heterodimeric enzyme with 92 and 29 kDa subunits. As in the other two Fdh enzymes, the catalytic subunit (92 kDa) includes the active site and one [4Fe-4S] centre (Fig. 8). The β subunit (29 kDa) contains three additional [4Fe-4S] centres involved in electron transfer. The overall fold of

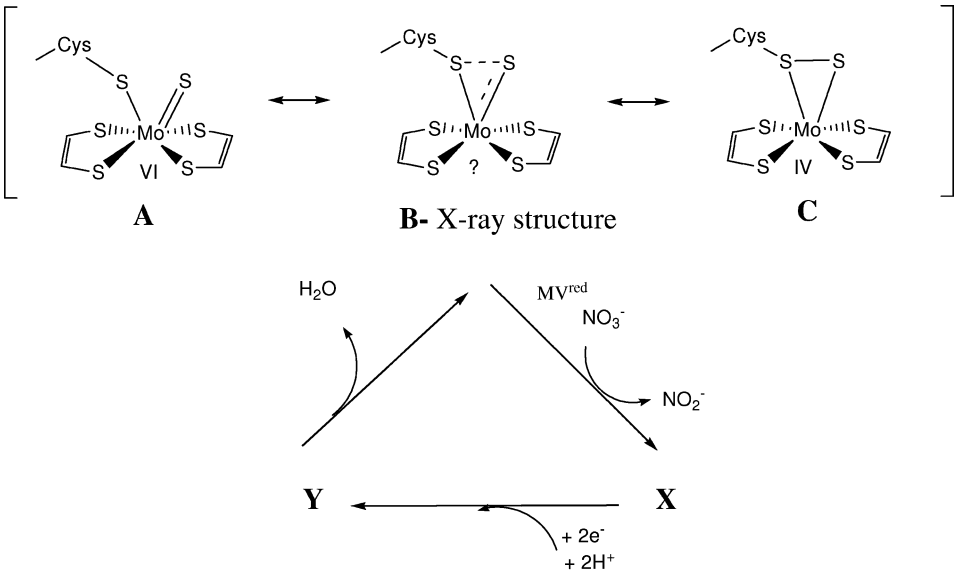

Possible alternative intermediates (**X**):

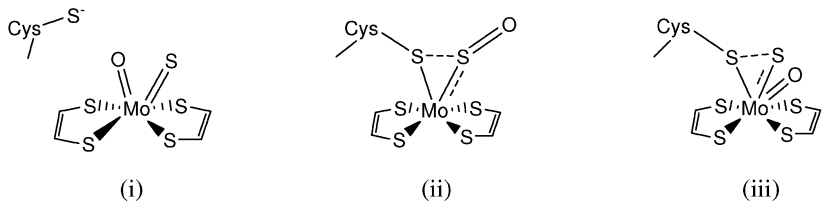

Scheme 5 Alternative reaction mechanisms for periplasmic nitrate reductases.[76] In the proposed mechanisms involving intermediates (i) or (iii), nitrate binds directly to the Mo atom, with the release of the Cys ligand (i) or forming an hepta-coordinated species (iii). In the proposed mechanism involving species (ii) reaction occurs on the second coordination sphere.

the catalytic subunit is similar to that of NapA and it can also be divided into four domains (I, II, III, and IV). The tungsten active site is buried inside the protein, accessible through a ~12 Å funnel. The W MGD cofactor is stabilized by hydrogen-bonding interactions to residues of mainly domains I, III, and IV. Domain I carries the characteristic cysteine motif that binds the first [4Fe-4S] centre.

The overall three-dimensional structure of all three Fdh proteins is very similar, as well as the relative arrangement of the cofactors. Residues at the active sites and surrounding area are also conserved.

The tungsten or molybdenum active site of FDH. In the active site of formate dehydrogenases, the W/Mo atom adopts a distorted trigonal prismatic geometry and is coordinated to four dithiolene sulfur atoms from the two MGDs, by the selenium atom of a conserved SeCys residue and by a sixth oxygen or sulfur ligand. (Fig. 9(a) and Table 2). This ligand was identified as a hydroxyl group in the X-ray structure of *E. coli* Fdh-N (1.6 Å resolution)[82] and *E. coli* Fdh-H (oxidized form, 2.8 Å resolution).[81] In contrast, the X-ray data of the tungsten-containing *D. gigas* Fdh (1.8 Å resolution) strongly suggested a sulfur atom for this coordination position.[20] Close to the Mo/W atom, there is a conserved His that establishes a π interaction with the Se atom of the metal ligand Se-Cys and occupies a similar position is all structures.

The three known structures of formate dehydrogenases (oxidized forms) exhibit very similar active site geometries (Mo or W). The only crystal structure available for a reduced Fdh is that of the formate-reduced *E. coli* Fdh-H[81,84] which revealed a penta-coordinated Mo active site, with the Se-Cys not bound to the Mo atom (Fig. 9-b).

Catalytic mechanism of formate dehydrogenase. The first proposal for the catalytic mechanism for the oxidation of formate to carbon dioxide was based on the first crystal structure of *E. coli* Fdh-H which was solved in oxidized (2.8 Å resolution) and formate-reduced (2.3 Å resolution) forms.[81] The mechanism then proposed involved the replacement of the hydroxyl group bound to the molybdenum by one of the oxygen atoms from formate followed by reduction of Mo(VI) to Mo(IV) and the cleavage of the C–H bond. However, an independent re-interpretation of the crystallographic data of the *E. coli* Fdh-H (formate-reduced form)[84] revealed important structural differences in relation to the published structure. This reanalysis showed that, for the reduced structure, an important loop at the active site (residues 139 to 146) was in a relatively weakly diffracting region and had therefore been mistraced. As a consequence catalytically relevant residues (SeCys140, His141, Arg138) were wrongly positioned. The most important result from the corrected structure was that selenocysteine 140, a ligand from molybdenum in the original

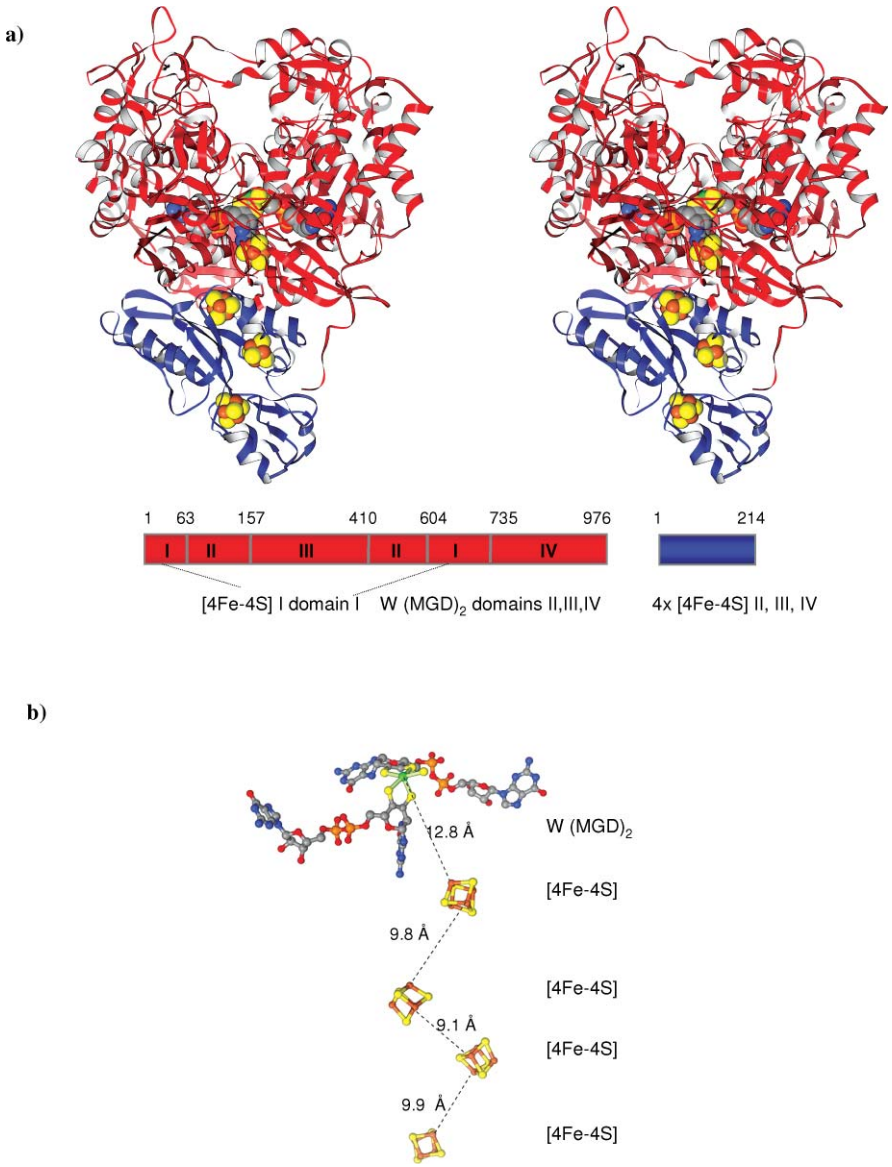

Fig. 8 (a) Stereo view of the crystal structure of the W-containing, heterodimeric *D. gigas* formate dehydrogenase[20,21] and schematic representation of the domain structure with respect to the primary sequence. (b) Arrangement of the five metal cofactors: W $(MGD)_2$, [4Fe-4S] I, [4Fe-4S] II, [4Fe-4S] III, [4Fe-4S] IV, colour-coded as atom types.

publication, is not bound after reduction with formate, being displaced 12 Å away from the molybdenum (Fig. 9-b). These results were not compatible with the original reaction mechanism which had to be revised (Scheme 6).[84]

In the new mechanistic proposal, the formate ion binds directly to the molybdenum atom, displacing SeCys140. The unbound negative selenol is stabilized by the proximity of Arg333 (Se–Nε1 3.5 Å). This Arg is a conserved residue and adopts different conformations in the oxidized and reduced forms of the Fdh structure. In the oxidized form (Fig. 9-a) it points towards the active site, orienting the formate molecule, while in the formate-reduced form Arg333 points away and is in contact with the free selenol from Se-Cys140 (Fig. 9-b). In the following step, the CO_2 molecule is released, two electrons are transferred to the molybdenum and a five-fold coordinated species is formed. Electrons are then transferred from Mo(IV) to the proximal [4Fe-4S] and the catalytic cycle is completed.

The crucial role of SeCys in the mechanism is in part supported by the fact that Fdh-H is completely inactivated by iodoacetamide after reduction with formate. In addition, this inactivation is pH-dependent and correlates with the pK_a value of ionized selenol.[85] In addition, this new mechanistic proposal is partly supported by EPR data on the Fdh from *D. desulfuricans*, which show that the SH ligand is retained in the Mo(V) state of the enzyme formed after CO_2 release.[68] These EPR studies suggest however that the structure of the molybdenum active site seems to depend on the enzyme preparation, and that several intermediate species could be involved in the mechanism of formate oxidation.

Recent density functional calculations were performed on a simplified model of formate dehydrogenase to investigate the two

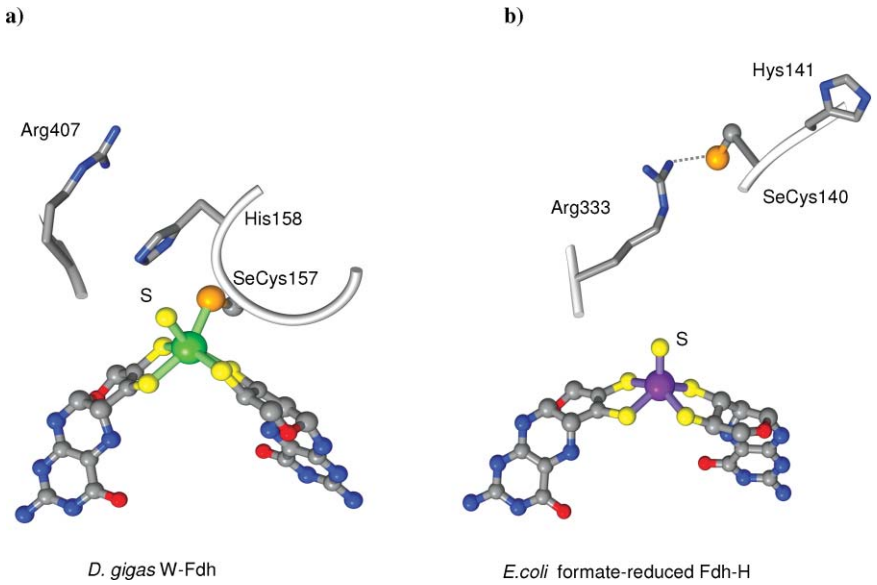

Fig. 9 (a) The W active site of *D. gigas* formate dehydrogenase [W-SeCys157,=S, $(MGD)_2$], and conserved residues His158 and Arg407 of the active site.[21] (b) The Mo active site of *E. coli* formate-reduced formate dehydrogenase [Mo,=S, $(MGD)_2$], with the SeCys140 ligand unbound (Mo–Se 12 Å).[84] The structure of the active site of the corresponding oxidized form (PDB code 1FDO) [Mo-SeCys140,=S/O,$(MGD)_2$][81] is superimposable with that from *D. gigas* W-Fdh (a).

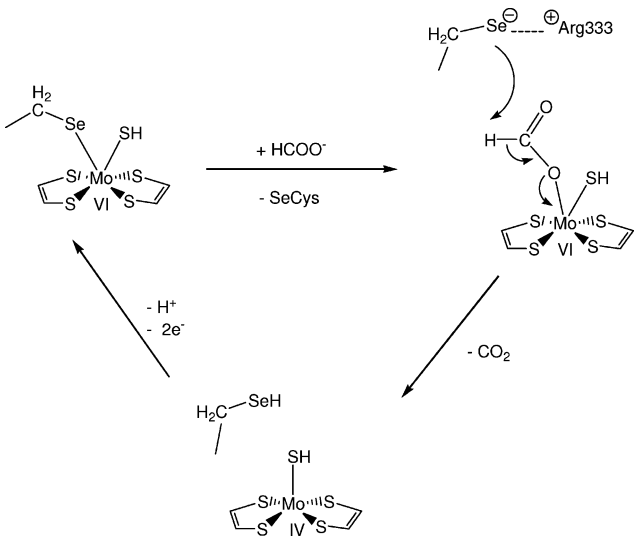

Scheme 6 Proposed reaction mechanism of formate dehydrogenases, based on the reanalyzed crystal structure of the formate-reduced *E. coli* Fdh-H[84] and supported by DFT calculations.[86]

alternative mechanisms, involving either a bound or an unbound SeCys residue.[86] The authors conclude that the oxidation of formate is kinetic and thermodynamically favored when the SeCys residue is in an unbound form and that this mechanism should be the preferred reaction pathway.

However, one should bear in mind that crystal structures correspond to the interpretation of electron density maps. With high resolution structures and adequate refinement and validation protocols, deposited structures are essentially correct. However, it is important to highlight that data interpretation is particularly sensitive for flexible or poorly defined regions in a structure.

3. Conclusions

The knowledge about molybdenum and tungsten pyranopterin-enzymes has increased rapidly, particularly due to the information obtained from high resolution crystal structures. The first two structures were reported in 1995, clarifying the true nature of the pyranopterin co-factor.[19,27] Since then the number of crystal structures has steadily increased. This growth in new crystal structures has been accompanied by a concomitant growth in new biochemical and spectroscopic information for these enzymes. Novel enzymes, some revealing new and unexpected functions, also continue to be discovered and characterized. Crystal structures have given insights into the pertinent electron transfer pathways and have revealed the atomic details of the enzymes active sites. This information, complemented by spectroscopic and kinetic data, has enabled detailed structure-based mechanistic studies to be performed. Expression systems are now available for producing fully functional recombinant enzymes, making it possible to explore the role of specific amino acid residues, thereby augmenting the mechanistic studies.

One can anticipate that the field of molybdenum and tungsten enzymes will continue to progress by the discovery and characterization of novel enzymes, by the determination of new crystal structures and by combining the information from complementary tools such as synthetic analogue studies, advanced spectroscopy, kinetics and computational studies.

Acknowledgements

The author thanks her many colleagues and friends from the Faculdade de Ciências e Tecnologia, Universidade Nova de Lisboa as well as from the Max-Planck Institut für Biochemie in Martinsried, with whom she has worked over the years on the field of molybdenum enzymes. In particular to José Moura,

Isabel Moura and their many co-workers for a long standing and fruitful collaboration, and to Robert Huber for all his support. José Trincão is gratefully acknowledged for preparing all the figures of this review as well as for many critical discussions. Thanks go also for Shabir Najmudin for critical reading of the manuscript. The author acknowledges the continuous financial help from the Portuguese Science and Technology Foundation (FCT-MCTES) through projects POCI/QUI/57641/2004 and PTDC/QUI/64733/2006 as well as several PhD and post-doctoral grants.

References

1 R. Hille, *Chem Rev*, 1996, **96**, 2757–2816.
2 R. Hille, *Met Ions Biol Syst*, 2002, **39**, 187–226.
3 Y. Zhang and V. N. Gladyshev, *J Mol Biol*, 2008, **379**, 881–899.
4 A. Kletzin and M. W. Adams, *FEMS Microbiol Rev*, 1996, **18**, 5–63.
5 M. K. Johnson, D. C. Rees and M. W. Adams, *Chem Rev*, 1996, **96**, 2817–2840.
6 J. R. Turnlund, *Met Ions Biol Syst*, 2002, **39**, 727–739.
7 C. Feng, G. Tollin and J. H. Enemark, *Biochim Biophys Acta*, 2007, **1774**, 527–539.
8 R. R. Mendel and R. Hansch, *J Exp Bot*, 2002, **53**, 1689–1698.
9 F. Lagarde and M. Leroy, *Met Ions Biol Syst*, 2002, **39**, 741–759.
10 E. Garattini, R. Mendel, M. J. Romao, R. Wright and M. Terao, *Biochemical J*, 2003, **372**, 15–32.
11 D. M. Lawson and B. E. Smith, *Met Ions Biol Syst*, 2002, **39**, 75–119.
12 R. M. Allen, R. Chatterjee, M. S. Madden, P. W. Ludden and V. K. Shah, *Crit Rev Biotechnol*, 1994, **14**, 225–249.
13 R. R. Mendel, *Dalton Trans*, 2005, 3404–3409.
14 R. R. Mendel and F. Bittner, *Biochim Biophys Acta*, 2006, **1763**, 621–635.
15 R. R. Mendel and G. Schwarz, *Met Ions Biol Syst*, 2002, **39**, 317–368.
16 H. Dobbek and R. Huber, *Met Ions Biol Syst*, 2002, **39**, 227–263.
17 M. J. Romao, J. Knablein, R. Huber and J. J. G. Moura, *Prog Biophys Mol Biol*, 1997, **68**, 121–144.
18 R. Roy and M. W. Adams, *Met Ions Biol Syst*, 2002, **39**, 673–697.
19 M. K. Chan, S. Mukund, A. Kletzin, M. W. Adams and D. C. Rees, *Science*, 1995, **267**, 1463–1469.
20 H. Raaijmakers, S. Macieira, J. M. Dias, S. Teixeira, S. Bursakov, R. Huber, J. J. G. Moura, I. Moura and M. J. Romao, *Structure*, 2002, **10**, 1261–1272.
21 H. Raaijmakers, S. Teixeira, J. M. Dias, M. J. Almendra, C. D. Brondino, I. Moura, J. J. G. Moura and M. J. Romao, *JBIC, J Biol Inorg Chem*, 2001, **6**, 398–404.
22 M. J. Romao and R. Huber, *Met Sites Proteins Models*, 1998, **90**, 69–95.
23 R. Hille, *E J Inorg Chem*, 2006, 1913–1926.
24 T. Nishino, K. Okamoto, B. T. Eger, E. F. Pai and T. Nishino, *FEBS J*, 2008, **275**, 3278–3289.
25 C. D. Brondino, M. J. Romao, I. Moura and J. J. Moura, *Curr Opin Chem Biol*, 2006, **10**, 109–114.
26 C. D. Brondino, M. G. Rivas, M. J. Romao, J. J. Moura and I. Moura, *Acc Chem Res*, 2006, **39**, 788–796.
27 M. J. Romao, M. Archer, I. Moura, J. J. Moura, J. LeGall, R. Engh, M. Schneider, P. Hof and R. Huber, *Science*, 1995, **270**, 1170–1176.
28 J. Rebelo, S. Macieira, J. M. Dias, R. Huber, C. S. Ascenso, F. Rusnak, J. J. G. Moura, I. Moura and M. J. Romao, *J Mol Biol*, 2000, **297**, 135–146.
29 H. Dobbek, L. Gremer, R. Kiefersauer, R. Huber and O. Meyer, *Proc Natl Acad Sci U S A*, 2002, **99**, 15971–15976.
30 P. Hanzelmann, H. Dobbek, L. Gremer, R. Huber and O. Meyer, *J Mol Biol*, 2000, **301**, 1221–1235.
31 I. Bonin, B. M. Martins, V. Purvanov, S. Fetzner, R. Huber and H. Dobbek, *Structure*, 2004, **12**, 1425–1435.
32 J. Johannes, M. C. Unciuleac, T. Friedrich, E. Warkentin, U. Ermler and M. Boll, *Biochemistry*, 2008, **47**, 4964–4972.
33 M. Unciuleac, E. Warkentin, C. C. Page, M. Boll and U. Ermler, *Structure*, 2004, **12**, 2249–2256.
34 D. R. Boer, A. Muller, S. Fetzner, D. J. Lowe and M. J. Romao, *Acta Crystallogr, Sect F: Struct Biol Cryst Commun*, 2005, **61**, 137–140.
35 R. Huber, P. Hof, R. O. Duarte, J. J. Moura, I. Moura, M. Y. Liu, J. LeGall, R. Hille, M. Archer and M. J. Romao, *Proc Natl Acad Sci U S A*, 1996, **93**, 8846–8851.
36 J. M. Rebelo, J. M. Dias, R. Huber, J. J. G. Moura and M. J. Romao, *JBIC, J Biol Inorg Chem*, 2001, **6**, 791–800.
37 C. Enroth, B. T. Eger, K. Okamoto, T. Nishino, T. Nishino and E. F. Pai, *Proc Natl Acad Sci U S A*, 2000, **97**, 10723–10728.
38 J. J. Truglio, K. Theis, S. Leimkuhler, R. Rappa, K. V. Rajagopalan and C. Kisker, *Structure*, 2002, **10**, 115–125.
39 H. Sticht and P. Rosch, *Prog Biophys Mol Biol*, 1998, **70**, 95–136.
40 K. Okamoto, B. T. Eger, T. Nishino, S. Kondo, E. F. Pai and T. Nishino, *J Biol Chem*, 2003, **278**, 1848–1855.
41 K. Okamoto, B. T. Eger, T. Nishino, E. F. Pai and T. Nishino, *Nucleosides Nucleotides Nucleic Acids*, 2008, **27**, 888–893.
42 K. Okamoto, K. Matsumoto, R. Hille, B. T. Eger, E. F. Pai and T. Nishino, *Proc Natl Acad Sci U S A*, 2004, **101**, 7931–7936.
43 J. M. Pauff, J. Zhang, C. E. Bell and R. Hille, *J Biol Chem*, 2008, **283**, 4818–4824.
44 Y. Yamaguchi, T. Matsumura, K. Ichida, K. Okamoto and T. Nishino, *J Biochem*, 2007, **141**, 513–524.
45 C. Kisker, H. Schindelin, A. Pacheco, W. A. Wehbi, R. M. Garrett, K. V. Rajagopalan, J. H. Enemark and D. C. Rees, *Cell*, 1997, **91**, 973–983.
46 R. Hansch, C. Lang, E. Riebeseel, R. Lindigkeit, A. Gessler, H. Rennenberg and R. R. Mendel, *J Biol Chem*, 2006, **281**, 6884–6888.
47 U. Kappler and S. Bailey, *J Biol Chem*, 2005, **280**, 24999–25007.
48 E. Karakas, H. L. Wilson, T. N. Graf, S. Xiang, S. Jaramillo-Buswuets, K. V. Rajagopalan and C. Kisker, *J Biol Chem*, 2005, **280**, 33506–33515.
49 N. Schrader, K. Fischer, K. Theis, R. R. Mendel, G. Schwarz and C. Kisker, *Structure*, 2003, **11**, 1251–1263.
50 K. Fischer, G. G. Barbier, H. J. Hecht, R. R. Mendel, W. H. Campbell and G. Schwarz, *Plant Cell*, 2005, **17**, 1167–1179.
51 A. Pacheco, J. T. Hazzard, G. Tollin and J. H. Enemark, *J Biol Inorg Chem*, 1999, **4**, 390–401.
52 C. Feng, R. V. Kedia, J. T. Hazzard, J. K. Hurley, G. Tollin and J. H. Enemark, *Biochemistry*, 2002, **41**, 5816–5821.
53 R. Hille, *Biochim Biophys Acta*, 1994, **1184**, 143–169.
54 C. A. McDevitt, P. Hugenholtz, G. R. Hanson and A. G. McEwan, *Mol Microbiol*, 2002, **44**, 1575–1587.
55 A. G. McEwan, J. P. Ridge, C. A. McDevitt and P. Hugenholtz, *Geomicrobiol J*, 2002, **19**, 3–21.
56 J. J. G. Moura, C. D. Brondino, J. Trincao and M. J. Romao, *JBIC, J Biol Inorg Chem*, 2004, **9**, 791–799.
57 M. G. Bertero, R. A. Rothery, M. Palak, C. Hou, D. Lim, F. Blasco, J. H. Weiner and N. C. Strynadka, *Nat Struct Biol*, 2003, **10**, 681–687.
58 M. Jormakka, D. Richardson, B. Byrne and S. Iwata, *Structure*, 2004, **12**, 95–104.
59 D. P. Kloer, C. Hagel, J. Heider and G. E. Schulz, *Structure*, 2006, **14**, 1377–1388.
60 F. Schneider, J. Lowe, R. Huber, H. Schindelin, C. Kisker and J. Knablein, *J Mol Biol*, 1996, **263**, 53–69.
61 H. Schindelin, C. Kisker, J. Hilton, K. V. Rajagopalan and D. C. Rees, *Science*, 1996, **272**, 1615–1621.
62 M. Czjzek, J. P. Dos Santos, J. Pommier, G. Giordano, V. Mejean and R. Haser, *J Mol Biol*, 1998, **284**, 435–447.
63 L. Zhang, K. J. Nelson, K. V. Rajagopalan and G. N. George, *Inorg Chem*, 2008, **47**, 1074–1078.
64 E. Lebrun, M. Brugna, F. Baymann, D. Muller, D. Lievremont, M. C. Lett and W. Nitschke, *Mol Biol Evol*, 2003, **20**, 686–693.
65 T. Conrads, C. Hemann, G. N. George, I. J. Pickering, R. C. Prince and R. Hille, *J Am Chem Soc*, 2002, **124**, 11276–11277.
66 P. J. Ellis, T. Conrads, R. Hille and P. Kuhn, *Structure*, 2001, **9**, 125–132.
67 G. B. Seiffert, G. M. Ullmann, A. Messerschmidt, B. Schink, P. M. Kroneck and O. Einsle, *Proc Natl Acad Sci U S A*, 2007, **104**, 3073–3077.
68 M. G. Rivas, P. J. Gonzalez, C. D. Brondino, J. J. Moura and I. Moura, *J Inorg Biochem*, 2007, **101**, 1617–1622.
69 J. F. Stolz and P. Basu, *ChemBioChem*, 2002, **3**, 198–206.
70 C. Moreno-Vivian, P. Cabello, M. Martinez-Luque, R. Blasco and F. Castillo, *J Bacteriol*, 1999, **181**, 6573–6584.
71 J. M. Dias, M. E. Than, A. Humm, R. Huber, G. P. Bourenkov, H. D. Bartunik, S. Bursakov, J. Calvete, J. Caldeira, C. Carneiro, J. J. Moura, I. Moura and M. J. Romao, *Structure*, 1999, **7**, 65–79.
72 P. Arnoux, M. Sabaty, J. Alric, B. Frangioni, B. Guigliarelli, J. M. Adriano and D. Pignol, *Nat Struct Biol*, 2003, **10**, 928–934.

73 B. J. Jepson, S. Mohan, T. A. Clarke, A. J. Gates, J. A. Cole, C. S. Butler, J. N. Butt, A. M. Hemmings and D. J. Richardson, *J Biol Chem*, 2007, **282**, 6425–6437.
74 C. Coelho, P. J. Gonzalez, J. Trincao, A. L. Carvalho, S. Najmudin, T. Hettman, S. Dieckman, J. J. G. Moura, I. Moura and M. J. Romao, *Acta Crystallogr, Sect F: Struct Biol Cryst Commun*, 2007, **63**, 516–519.
75 T. Hettmann, R. A. Siddiqui, J. von Langen, C. Frey, M. J. Romao and S. Diekmann, *Biochem Biophys Res Commun*, 2003, **310**, 40–47.
76 S. Najmudin, P. J. Gonzalez, J. Trincao, C. Coelho, A. Mukhopadhyay, N. M. F. S. A. Cerqueira, C. C. Romao, I. Moura, J. J. G. Moura, C. D. Brondino and M. J. Romao, *JBIC, J Biol Inorg Chem*, 2008, **13**, 737–753.
77 J. M. Berg, D. J. Spira, K. O. Hodgson, A. E. Bruce, K. F. Miller, J. L. Corbin and E. I. Stiefel, *Inorg Chem*, 1984, **23**, 3412–3418.
78 E. I. Stiefel, K. F. Miller, A. E. Bruce, J. L. Corbin, J. M. Berg and K. O. Hodgson, *J. Am. Chem. Soc.*, 1980, **102**, 3624–3626.
79 P. J. Gonzalez, M. G. Rivas, C. D. Brondino, S. A. Bursakov, I. Moura and J. J. Moura, *JBIC, J Biol Inorg Chem*, 2006, **11**, 609–616.
80 C. S. Butler, J. M. Charnock, B. Bennett, H. J. Sears, A. J. Reilly, S. J. Ferguson, C. D. Garner, D. J. Lowe, A. J. Thomson, B. C. Berks and D. J. Richardson, *Biochemistry*, 1999, **38**, 9000–9012.
81 J. C. Boyington, V. N. Gladyshev, S. V. Khangulov, T. C. Stadtman and P. D. Sun, *Science*, 1997, **275**, 1305–1308.
82 M. Jormakka, S. Tornroth, B. Byrne and S. Iwata, *Science*, 2002, **295**, 1863–1868.
83 M. Jormakka, B. Byrne and S. Iwata, *Curr Opin Struct Biol*, 2003, **13**, 418–423.
84 H. C. A. Raaijmakers and M. J. Romao, *JBIC, J Biol Inorg Chem*, 2006, **11**, 849–854.
85 M. J. Axley, A. Bock and T. C. Stadtman, *Proc Natl Acad Sci U S A*, 1991, **88**, 8450–8454.
86 M. Leopoldini, S. G. Chiodo, M. Toscano and N. Russo, *Chemistry*, 2008, **14**, 8674–8681.